A New 2D Analytic Threshold-Voltage Model for Fully Depleted Short-Channel SOI MOSFET's

Jwin-Yen Guo, *Student Member, IEEE,* and Ching-Yuan Wu, *Member, IEEE*

***Abstract*—The exact solution of the 2D Poisson's equation for the fully depleted SOI MOSFET's is derived by using a three-zone Green's function solution technique. Based on the derived 2D potential distribution, the front and back surface potential distributions in the Si film are analytically obtained and their accuracy are verified by 2D numerical analysis. The calculated minimum surface potential and its location are used to analyze the drain-induced barrier-lowering effect and further to develop an analytic threshold-voltage model. Comparisons between the developed analytic threshold-voltage model and the 2D numerical analysis are made. It is shown that excellent agreements are obtained for wide ranges of device structure parameters and applied biases.**

Nomenclature

$\epsilon_{si}(\epsilon_{ox})$	Dielectric permittivity of Si (SiO_2).
q	Elementary charge.
n_i	Intrinsic carrier concentration of semiconductor.
t_{si}	Thickness of Si film.
$t_{of}(t_{ob})$	Thickness of front (bottom)-gate oxide.
L	Effective channel length.
k_n^i	Eigenvalue of Region $i(i$ = I, II, III) ($k_n^I = [n - 1/2]\pi/t_{of}$ for Region I, $k_n^{II} = n\pi/t_{si}$ for Region II, and $k_n^{III} = [n - 1/2]\pi/t_{ob}$ for Region III).
k_m	Eigenvalue in all regions ($k_m = m\pi/L$).
$N_B f(y)$	Doping profile in the Si film, where $f(y)$ is a doping profile function with $f(y) = 1$ for uniform doping concentration.
$V_{bi}(y)$	Built-in potential of the source(drain)/body junctions in Region II.
V_{gs}	Gate–source voltage.
V_{ds}	Drain–source voltage.
V_{BS}	Back gate–source voltage.
$V_{fb,f}(V_{fb,b})$	Flatband voltage of the front (back) gate.
$V'_{gs}(V'_{BS})$	$= V_{gs} - V_{fb,f}(V_{BS} - V_{fb,b})$.
$D_{sf}(x)(D_{sb}(x))$	Electric displacement at the front (back) Si–SiO_2 interface.
$\Phi^i(x, y)$	2D potential distribution in Region i (i = I, II, III).
$E_y^i(x, y)$	2D vertical electric field distribution in Region $i(i$ = I, II, III).
$\Phi_f^{II}(x)(\Phi_b^{II}(x))$	Front (back) surface potential in Region II.
$Q_B^n(Q_B^0)$	Fourier coefficient of the bulk charge density with the integer $n(n = 0)$ in Region II

$$Q_B^n = \frac{2}{t_{si}} \int_0^{t_{si}} (-qN_B) f(y) \cos k_n^{II} y \, dy$$

and

$$Q_B^0 = \frac{1}{t_{si}} \int_0^{t_{si}} (-qN_B) f(y) \, dy$$

$D_{sf}^m(D_{sb}^m)$ Fourier coefficient of the electric displacement at the front (back) surface

$$D_{sf}^m = \frac{2}{L} \int_0^L D_{sf}(x) \sin k_m x \, dx$$

$$D_{sb}^m = \frac{2}{L} \int_0^L D_{sb}(x) \sin k_m x \, dx$$

$A_n^s(A_n^d)$ Fourier coefficient of the boundary potential at the source (drain) side in Region I

$$A_n^s = \frac{2}{t_{of}} \int_0^{t_{of}} \phi^I(0, y) \cos k_n^I y \, dy$$

and

$$A_n^d = \frac{2}{t_{of}} \int_0^{t_{of}} \phi^I(L, y) \cos k_n^I y \, dy.$$

$B_n^s(B_0^s)$ Fourier coefficient of the source boundary potential with the integer n ($n = 0$) in Region II

$$B_n^s = \frac{2}{t_{si}} \int_0^{t_{si}} V_{bi}(y) \cos k_n^{II} y \, dy$$

and

$$B_0^s = \frac{1}{t_{si}} \int_0^{t_{si}} V_{bi}(y) \, dy$$

Manuscript received October 5, 1992; revised March 1, 1993. This work was supported by the National Science Council, Taiwan, ROC, under Grant NSC81-0404-E-009-139. J. Y. Guo was supported by the Electronic Research and Service Organization (ERSO), ITRI, under a special research scholarship. The review of this paper was arranged by Associate Editor D. A. Antoniadis.

The authors are with Advanced Semiconductor Device Research Laboratory and the Institute of Electronics, National Chiao-Tung University, Hsinchu, Taiwan, ROC.

IEEE Log Number 9210619.

$B_n^d(B_0^d)$ Fourier coefficient of the drain boundary potential with the integer n ($n = 0$) in Region II

$$B_n^d = \frac{2}{t_{si}} \int_0^{t_{si}} [V_{bi}(y) + V_{ds}] \cdot \cos k_n^{II} y \, dy$$

and

$$B_0^d = \frac{1}{t_{si}} \int_0^{t_{si}} [V_{bi}(y) + V_{ds}] \, dy.$$

$C_n^s(C_n^d)$ Fourier coefficient of the boundary potential at the source (drain) side in Region III

$$C_n^s = \frac{2}{t_{ob}} \int_0^{t_{ob}} \phi^{III}(0, y) \cos k_n^{III} y \, dy$$

and

$$C_n^d = \frac{2}{t_{ob}} \int_0^{t_{ob}} \phi^{III}(L, y) \cos k_n^{III} y \, dy.$$

$\phi_{f,\text{inv}}$ Front surface potential at strong inversion condition

$$\phi_{f,\text{inv}} = 2\phi_{fp}$$

and

$$\phi_{fp} = \frac{k_B T}{q} \cdot \ln\left(\frac{N_B}{n_i}\right)$$

$x_{\min}$ Location of the minimum surface potential at the front Si surface.

I. Introduction

THE MOSFET device fabricated on a thin SOI film and operated in the fully depleted mode has shown to have smaller drain-induced barrier-lowering effect [1] and higher punchthrough voltage [2] when compared to those of bulk MOSFET's. Moreover, its inherent advantages of latch-up-free and high-speed operation may give the best solution to many submicrometer CMOS problems [3]. However, the coupling effects between the front and back gates become complicated for short-channel SOI MOSFET devices. Therefore, it is difficult to derive a simple and accurate model for device design and circuit analysis.

The analytical modeling of short-channel SOI MOSFET's had been reported by several authors [4]–[7]. Veeraraghavan and Fossum [4] used a conventional charge-sharing scheme to develop the threshold-voltage model for the I–V characteristics. Young [5] assumed a trial function with a parabolic-like potential distribution for the 2D Poisson's equation and developed an analytic model for the drain-induced barrier lowering. This simplified assumption underestimates the effects of the source/drain junctions and may cause significant error when the channel length of the device is very short. Moreover, the effect of the nonuniformly doped profile in the Si film cannot be taken into account by this kind of analysis. Recently, based on the analysis of Ratnakumar and Meindl [6], Woo *et al.* [7] separated the 2D Poisson's equation into a 1D Poisson's equation and a 2D Laplace equation. Moreover, the continuity of the electric field across the Si–bottom oxide interface was assumed instead of the continuity of the electric displacement. This assumption may cause a large error for short-channel SOI MOSFET's and an additional series is introduced to improve the accuracy of the potential distribution. Due to the complicated 2D potential distribution, it was difficult for Woo *et al.* [7] to derive an analytic threshold-voltage model for short-channel SOI MOSFET's.

In order to analytically model the 2D characteristics of short-channel thin film SOI MOSFET's, the 2D Poisson's equation must be solved by incorporating the suitable boundary conditions. The Green's function technique may give an exact solution for the 2D Poisson's equation including the nonuniform doping profile. This advantage was first demonstrated in solving the 2D potential distribution of a bulk MOSFET by Lin and Wu [8]. Recently, the multizone solution using the Green's function technique has been successfully used to describe the electrical characteristics of short gate-length MESFET's by Chin and Wu [9]. In order to avoid the complexity in dealing with the equivalent charge densities between the regions of different dielectric materials, the multizone solutions with mixed boundary conditions are used in this work to analytically solve the 2D Poisson's equation in three regions with different dielectrics.

In Section II, the Green's function solution technique for solving the 2D Poisson's equation in all regions is introduced and the boundary conditions corresponding to each region are also described. The analytic 2D potential distribution in the silicon region is derived exactly and verified by 2D numerical analysis. In Section III, the derived 2D potential distribution is further used to develop the threshold-voltage model, in which the drain-induced barrier lowering is calculated by the derived 2D potential distribution. In addition, the results of the derived threshold-voltage model are compared with those of 2D numerical analysis. It is shown that excellent agreement between the developed threshold-voltage model and the 2D numerical analysis are obtained, and these verify the applicability of the boundary conditions used in our analysis. At last, a concluding remark is given in Section IV.

II. The Basic Analysis

The basic structure of a thin-film SOI MOSFET for 2D numerical simulation is shown in Fig. 1, where the simplified domain for analytically solving the 2D Poisson's equation is highlighted by the bolded lines and the boundary conditions used are also listed. In order to avoid the complexity in calculating the equivalent charge density between the regions of different dielectrics, the domain for solving the 2D Poisson's equation is further divided

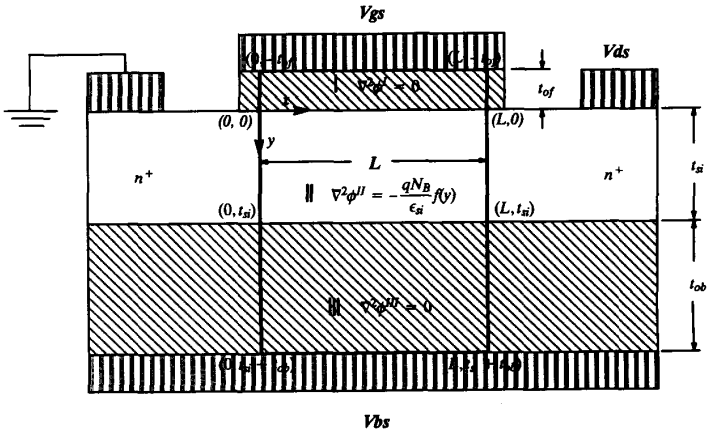

$$\phi^I(x, -t_{of}) = V_{gs} - V_{fb,f} = V_{gs}'$$
$$\phi^I(0, y) = V_{bi}(0) + \frac{V_{bi}(0) - V_{gs}'}{t_{of}} y$$
$$\phi^I(L, y) = V_{bi}(0) + V_{ds} + \frac{V_{bi}(0) + V_{ds} - V_{gs}'}{t_{of}} y$$
$$\epsilon_{ox} E_y^I(x, 0) = \epsilon_{si} E_y^{II}(x, 0) = D_{sf}(x)$$
$$\phi^{II}(0, y) = V_{bi}(y)$$
$$\phi^{II}(L, y) = V_{bi}(y) + V_{ds}$$
$$\epsilon_{si} E_y^{II}(x, t_{si}) = \epsilon_{ox} E_y^{III}(x, t_{si}) = D_{sb}(x)$$
$$\phi^{III}(x, t_{si} + t_{ob}) = V_{BS} - V_{fb,b} = V_{BS}'$$
$$\phi^{III}(0, y) = V_{bi}(t_{si}) - \frac{V_{bi}(t_{si}) - V_{BS}'}{t_{ob}} (y - t_{si})$$
$$\phi^{III}(L, y) = V_{bi}(t_{si}) + V_{ds} - \frac{V_{bi}(t_{si}) + V_{ds} - V_{BS}'}{t_{ob}} (y - t_{si})$$

Fig. 1. The basic cross-sectional view of a thin-film SOI MOSFET device structure with the listed boundary conditions.

into three subdomains, as shown in Fig. 1, in which Region I is the front gate-oxide region; Region II represents the Si film; and Region III is the bottom oxide region. Note that the boundary potentials in the y direction in Regions I and III are assumed to vary linearly [7]. The possible errors caused by these assumptions will be discussed later. It is noted that the effects of impact ionization are neglected for simplicity.

Although the 2D Poisson's equations in the front and back oxide regions are reduced to the 2D Laplace equations, the Green's function solution technique is still implemented to solve the 2D potential distribution. Due to different types of boundary conditions and geometries of the regions, the Green's function solution in each region is used and summarized in Table I.

Substituting the Green's function solutions listed in Table I into the Green's theorem [9] and neglecting the free carriers, the general form of the 2D potential distribution in each region can be derived as follows:

$$\Phi^I(x, y) = \sum_{m=\text{odd}}^{\infty} \frac{4V_{gs}'}{m\pi} \frac{\cosh k_m y}{\cosh k_m t_{of}} \sin k_m x - \sum_{m=1}^{\infty} \frac{D_{sf}^m}{\epsilon_{ox}} \frac{\sinh k_m (t_{of} + y)}{k_m \cosh k_m t_{of}} \sin k_m x + \sum_{n=1}^{\infty} \frac{\cos k_n^I y}{\sinh k_n^I L} [A_n^s \sinh k_n^I (L - x) + A_n^d \sinh k_n^I x] \quad (1)$$

$$\Phi^{II}(x, y) = \frac{Q_B^0}{2\epsilon_{si}} x(L - x) + \sum_{n=1}^{\infty} \frac{Q_B^n}{\epsilon_{si}} \frac{\cos k_n^{II} y}{(k_n^{II})^2} \cdot \left[1 - \frac{\sinh k_n^{II} x + \sinh k_n^{II} (L - x)}{\sinh k_n^{II} L}\right] + B_0^s \left(1 - \frac{x}{L}\right) + B_0^d \frac{x}{L} + \sum_{n=1}^{\infty} \frac{\cos k_n^{II} y}{\sinh k_n^{II} L} [B_n^s \sinh k_n^{II} (L - x) + B_n^d \sinh k_n^{II} x] + \sum_{m=1}^{\infty} \frac{\sin k_m x}{\epsilon_{si} k_m \sinh k_m t_{si}} [D_{sf}^m \cosh k_m (t_{si} - y) - D_{sb}^m \cosh k_m y] \quad (2)$$

$$\Phi^{III}(x, y) = \sum_{m=\text{odd}}^{\infty} \frac{4V_{BS}'}{m\pi} \frac{\cosh k_m (y - t_{si})}{\cosh k_m t_{ob}} \sin k_m x + \sum_{m=1}^{\infty} \frac{D_{sb}^m}{\epsilon_{ox}} \frac{\sinh k_m (t_{ob} - y + t_{si})}{k_m \cosh k_m t_{ob}} \sin k_m x + \sum_{n=1}^{\infty} \frac{\cos k_n^{III} (y - t_{si})}{\sinh k_n^{III} L} [C_n^s \sinh k_n^{III} (L - x) + C_n^d \sinh k_n^{III} x] \quad (3)$$

where the Fourier coefficients have been given in the Nomenclature.

Differentiating $\Phi^I(x, y)$ and $\Phi^{II}(x, y)$ with respect to y

TABLE I
THE GREEN FUNCTION SOLUTION FOR DIFFERENT REGIONS

Region I	$G_x^{\mathrm{I}}(x, y; x', y') = \frac{2}{L}\sum_{m=1}^{\infty} \sin k_m x \sin k_m x' \frac{\cosh k_m y \sinh k_m(t_{of} + y')}{k_m \cosh k_m t_{of}}$	$y' < y$
	$G_x^{\mathrm{I}}(x, y; x', y') = \frac{2}{L}\sum_{m=1}^{\infty} \sin k_m x \sin k_m x' \frac{\cosh k_m y' \sinh k_m(t_{of} + y)}{k_m \cosh k_m t_{of}}$	$y < y'$
	$G_y^{\mathrm{I}}(x, y; x', y') = \frac{2}{t_{of}}\sum_{n=1}^{\infty} \cos k_n^{\mathrm{I}} y \cos k_n^{\mathrm{I}} y' \frac{\sinh k_n^{\mathrm{I}} x \sinh k_n^{\mathrm{I}}(L - x')}{k_n^{I} \sinh k_n^{\mathrm{I}} L}$	$x < x'$
	$G_y^{\mathrm{I}}(x, y; x', y') = \frac{2}{t_{of}}\sum_{n=1}^{\infty} \cos k_n^{\mathrm{I}} y \cos k_n^{\mathrm{I}} y' \frac{\sinh k_n^{\mathrm{I}} x' \sinh k_n^{\mathrm{I}}(L - x)}{k_n^{I} \sinh k_n^{\mathrm{I}} L}$	$x' < x$
Region II	$G_x^{\mathrm{II}}(x, y; x', y') = \frac{2}{L}\sum_{m=1}^{\infty} \sin k_m x \sin k_m x' \frac{\cosh k_m y \cosh k_m(t_{\mathrm{si}} - y')}{k_m \sinh k_m t_{\mathrm{st}}}$	$y' < y$
	$G_x^{\mathrm{II}}(x, y; x', y') = \frac{2}{L}\sum_{m=1}^{\infty} \sin k_m x \sin k_m x' \frac{\cosh k_m y' \cosh k_m(t_{\mathrm{si}} - y)}{k_m \sinh k_m t_{\mathrm{si}}}$	$y < y'$
	$G_y^{\mathrm{II}}(x, y; x', y') = \frac{c}{t_{\mathrm{si}}}\sum_{n=0}^{\infty} \cos k_n^{\mathrm{II}} y \cos k_n^{\mathrm{II}} y' \frac{\sinh k_n^{\mathrm{II}} x \sinh k_n^{\mathrm{II}}(L - x')}{k_n^{\mathrm{II}} \sinh k_n^{\mathrm{II}} L}$	$x < x'$
	$G_y^{\mathrm{II}}(x, y; x', y') = \frac{c}{t_{\mathrm{si}}}\sum_{n=0}^{\infty} \cos k_n^{\mathrm{II}} y \cos k_n^{\mathrm{II}} y' \frac{\sinh k_n^{\mathrm{II}} x' \sinh k_n^{\mathrm{II}}(L - x)}{k_n^{\mathrm{II}} \sinh k_n^{\mathrm{II}} L}$	$x' < x$
	$c = 1$, for $n = 0$	
	$c = 2$, for $n > 0$	
Region III	$G_x^{\mathrm{III}}(x, y; x', y') = \frac{2}{L}\sum_{m=1}^{\infty} \sin k_m x \sin k_m x' \frac{\cosh k_m(y - t_{\mathrm{si}}) \sinh k_m(t_{ob} + t_{\mathrm{si}} - y')}{k_m \cosh k_m t_{ob}}$	$y' < y$
	$G_x^{\mathrm{III}}(x, y; x', y') = \frac{2}{L}\sum_{m=1}^{\infty} \sin k_m x \sin k_m x' \frac{\cosh k_m(y' - t_{\mathrm{si}}) \sinh k_m(t_{ob} + t_{\mathrm{si}} - y)}{k_m \cosh k_m t_{ob}}$	$y < y'$
	$G_y^{\mathrm{III}}(x, y; x', y') = \frac{2}{t_{ob}}\sum_{n=1}^{\infty} \cos k_n^{\mathrm{III}}(y - t_{\mathrm{st}}) \cos k_n^{\mathrm{III}}(y' - t_{\mathrm{si}}) \frac{\sinh k_n^{\mathrm{III}} x \sinh k_n^{\mathrm{III}}(L - x')}{k_n^{\mathrm{III}} \sinh k_n^{\mathrm{III}} L}$	$x < x'$
	$G_y^{\mathrm{III}}(x, y; x', y') = \frac{2}{t_{ob}}\sum_{n=1}^{\infty} \cos k_n^{\mathrm{III}}(y - t_{\mathrm{st}}) \cos k_n^{\mathrm{III}}(y' - t_{\mathrm{si}}) \frac{\sinh k_n^{\mathrm{III}} x \sinh k_n^{\mathrm{III}}(L - x)}{k_n^{\mathrm{III}} \sinh k_n^{\mathrm{III}} L}$	$x' < x$

at $y = 0$ and $\Phi^{\mathrm{II}}(x, y)$ and $\Phi^{\mathrm{III}}(x, y)$ with respect to y at $y = t_{\mathrm{si}}$, we obtain the continuities of the electric displacement at the two Si–SiO_2 interfaces ($y = 0$ and $y = d$), and the complexity of dealing with the equivalent charge densities at the interfaces is thus avoided. To obtain the exact potential distribution, D_{sf}^m and D_{sb}^m have to be solved first. By equating (1) and (2) at $y = 0$ and (2) and (3) at $y = t_{\mathrm{si}}$, D_{sf}^m and D_{sb}^m can be obtained. Note that the above equations are exact and the arbitrary doping profile in the Si film can be treated. It is clearly seen that the second term on the right-hand side of (2) demonstrates the charge-coupling effect between the boundaries of source and drain sides, which was overlooked in [7].

In the following analysis, the uniformly doped Si film is assumed for simplicity. In this case, $f(y) = 1$, and the Fourier coefficients (Q_B^n, B_n^s, and B_n^d) would vanish except for $n = 0$, i.e., $Q_B^0 = -qN_B$, $B_0^s = V_{bi}$, and $B_0^d = V_{bi} + V_{ds}$. The 2D potential distribution in Region II is our major concern and can be written as

$$\Phi^{\mathrm{II}}(x, y) = -\frac{qN_B}{2\epsilon_{si}} x(L - x) + V_{bi} + \frac{x}{L} \cdot V_{ds} + \sum_{m=1}^{\infty} \frac{\sin k_m x}{\epsilon_{\mathrm{si}} k_m \sinh k_m t_{\mathrm{si}}} [D_{sf}^m \cosh k_m(t_{\mathrm{si}} - y) - D_{sb}^m \cosh k_m y] \quad (4)$$

where D_{sf}^m and D_{sb}^m have been deduced by equating (4) and (1) at $y = 0$ and (4) and (3) at $y = t_{\mathrm{si}}$, which are expressed as

$$D_{sf}^m = \frac{\epsilon_{\mathrm{si}} k_m}{d_0^m}\left[\frac{d_2^m}{\sinh k_m t_{\mathrm{si}}} - d_1^m\left(\frac{1}{\tanh k_m t_{\mathrm{si}}} + \frac{\epsilon_{\mathrm{si}}}{\epsilon_{\mathrm{ox}}} \cdot \tanh k_m t_{ob}\right)\right]$$

$$D_{sb}^m = \frac{\epsilon_{\mathrm{si}} k_m}{d_0^m}\left[d_2^m\left(\frac{1}{\tanh k_m t_{\mathrm{si}}} + \frac{\epsilon_{\mathrm{si}}}{\epsilon_{\mathrm{ox}}} \tanh k_m t_{of}\right) - \frac{d_1^m}{\sinh k_m t_{\mathrm{si}}}\right]$$

in which

$$d_1^m = -\phi_q^m + \frac{2V'_{gs}}{m\pi} \frac{1 - (-1)^m}{\cosh k_m t_{of}} + h_m^{\mathrm{I}}$$

$$d_2^m = -\phi_q^m + \frac{2V'_{BS}}{m\pi} \frac{1 - (-1)^m}{\cosh k_m t_{ob}} + h_m^{\mathrm{III}}$$

$$\phi_q^m = \frac{2}{m\pi}\left[(1 - (-1)^m)\left(-\frac{qN_B}{\epsilon_{si}}\right) + (1 - (-1)^m)V_{bi} + (-1)^{m+1} V_{ds}\right]$$

$$h_m^{\mathrm{I}} = \sum_{n=1}^{\infty} 0.5\, t_{mn}^{\mathrm{I}}[A_n^s + (-1)^{m+1}A_n^d]$$

$$h_m^{\mathrm{III}} = \sum_{n=1}^{\infty} 0.5\, t_{mn}^{\mathrm{III}}[C_n^s + (-1)^{m+1}C_n^d]$$

$$t_{mn}^{\mathrm{I}} = \frac{4}{m\pi}\left[1 + \frac{L^2(n-0.5)^2}{t_{of}^2 m^2}\right]^{-1}$$

$$t_{mn}^{\mathrm{III}} = \frac{4}{m\pi}\left[1 + \frac{L^2(n-0.5)^2}{t_{ob}^2 m^2}\right]^{-1}$$

$$d_0^m = \frac{1}{(\sinh k_m t_{\mathrm{si}})^2} - \left(\frac{1}{\tanh k_m t_{\mathrm{si}}} + \frac{\epsilon_{\mathrm{si}}}{\epsilon_{\mathrm{ox}}}\tanh k_m t_{of}\right) \cdot \left(\frac{1}{\tanh k_m t_{\mathrm{si}}} + \frac{\epsilon_{\mathrm{si}}}{\epsilon_{\mathrm{ox}}}\tanh k_m t_{ob}\right).$$

From (4), the potential distribution along the front surface of Si film can be obtained as

$$\Phi_f^{\mathrm{II}}(x) = -\frac{qN_B}{2\epsilon_{\mathrm{si}}}x(L-x) + V_{bi} + \frac{x}{L}V_{ds} + \sum_{m=1}^{\infty}\frac{\sin k_m x}{\epsilon_{\mathrm{si}}k_m \sinh k_m t_{\mathrm{si}}}(D_{sf}^m \cosh k_m t_{\mathrm{si}} - D_{sb}^m). \tag{5}$$

In order to check the accuracy of the derivations, the calculated results using (5) are compared with those calculated by a 2D numerical simulator [10], in which a new discretized Green's theorem was implemented in the simulator to directly solve the Poisson's equations in different dielectric regions and the finite difference scheme was used to discretize the current continuity equations in the semiconductor region.

Fig. 2(a) shows the calculated front surface potential as a function of the normalized distance from the source edge with the effective channel length as a normalization parameter. It is clearly seen that excellent agreements can be obtained even for a device with the effective channel length as short as 0.3 μm. Note that the number of terms (m) used in (5) can be as small as 10 to attain such an accuracy. Moreover, the calculated results using Young's model [5] are also shown by the dashed lines in the figure for comparisons. It is clearly seen that the parabolic potential distribution along the y direction is insufficient to describe the effects of the source(drain)/body junctions for short-channel SOI MOSFET's. Obviously, the model developed by Young [5] underestimates the drain-induced barrier-lowering effect. Similarly, the back surface potential can also be obtained from (4) and is expressed by

$$\Phi_b^{\mathrm{II}}(x) = -\frac{qN_B}{2\epsilon_{\mathrm{si}}}x(L-x) + V_{bi} + \frac{x}{L}V_{ds} + \sum_{m=1}^{\infty}\frac{\sin k_m x}{\epsilon_{\mathrm{si}}k_m \sinh k_m t_{\mathrm{si}}}(D_{sf}^m - D_{sb}^m \cosh k_m t_{\mathrm{si}}). \tag{6}$$

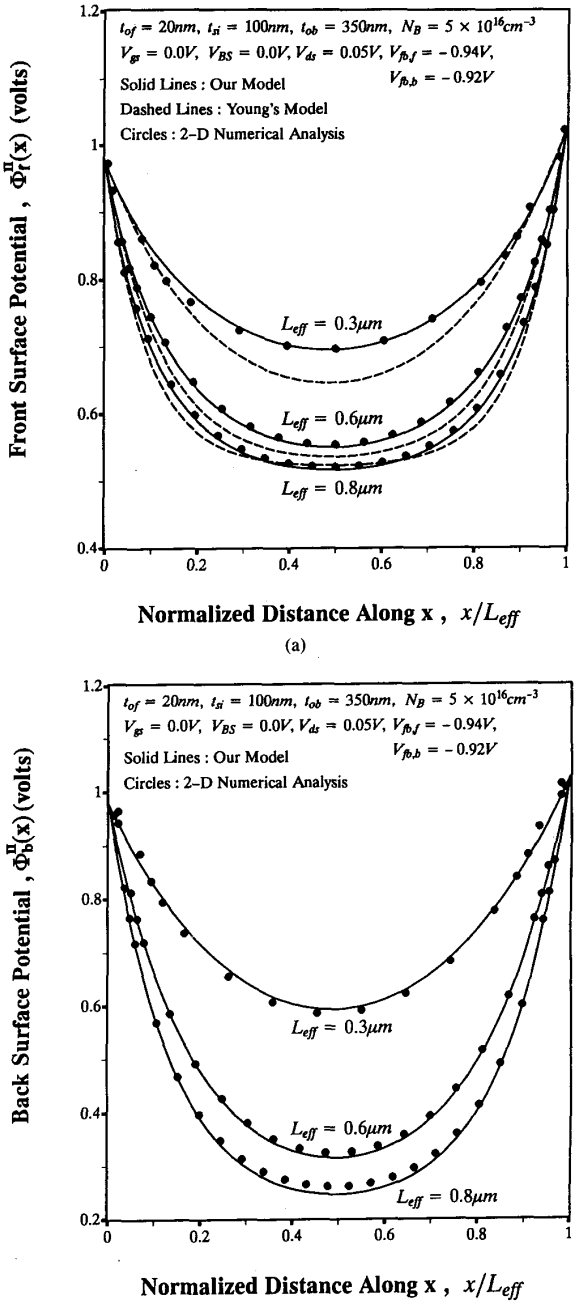

Fig. 2. The surface potential as a function of the normalized distance from the source edge with the effective channel length as a normalization parameter (a) Front surface potential. (b) Back surface potential.

The back surface potential as a function of the normalized distance from the source edge with the effective channel length as a normalization parameter is shown in Fig. 2(b). It is clearly seen that excellent agreements between (6) and 2D numerical analysis are also obtained. The effects of the drain bias are shown in Fig. 3, in which Fig. 3(a) shows the front and back surface potentials of a device

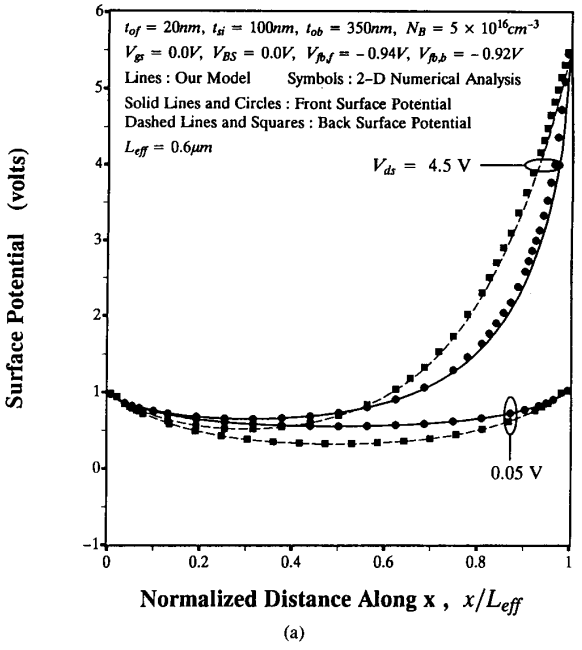

(a)

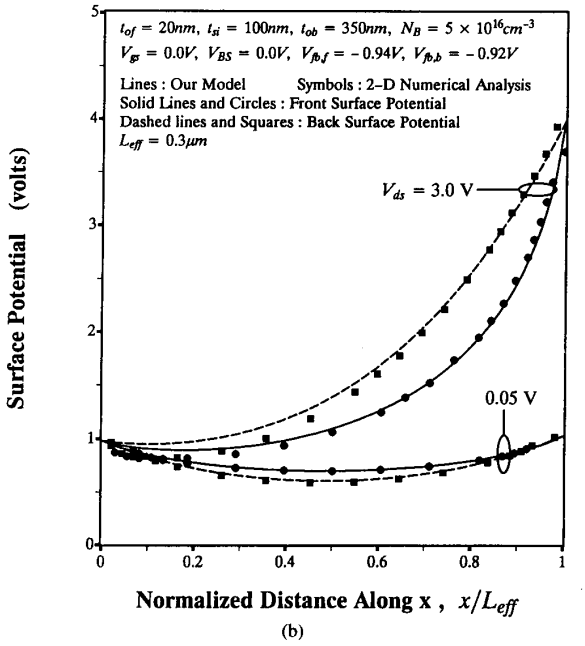

(b)

Fig. 3. The surface potential as a function of the normalized distance from the source edge with the drain bias as a parameter (a) Front and back surface potentials for a 0.6-μm SOI MOSFET operated with different drain biases from 0.05 to 4.5 V. (b) Front and back surface potentials for a 0.3-μm SOI MOSFET operated with different drain biases from 0.05 to 3.0 V.

with $L_{\text{eff}} = 0.6$ μm; and Fig. 3(b) shows the case with $L_{\text{eff}} = 0.3$ μm. It is clearly seen that good agreements between our analytic model and 2D numerical analysis are also obtained. Comparison of the calculated vertical potential distribution (y-direction) at the minimum surface potential point between our model and 2D numerical analysis for different channel lengths and drain biases are

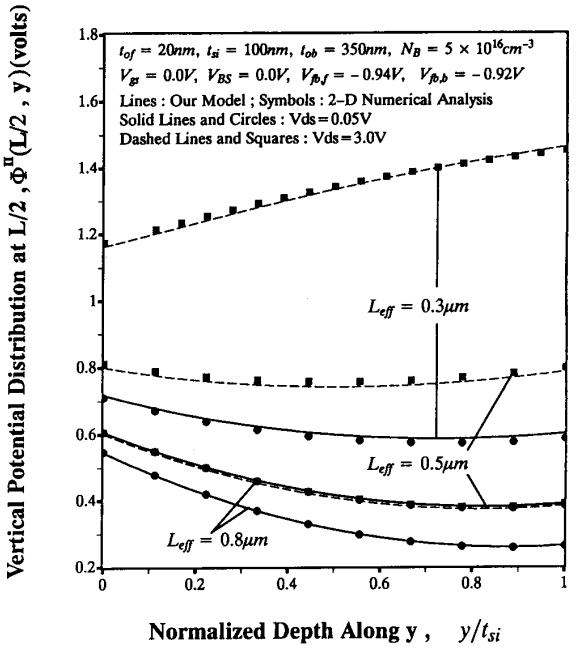

Fig. 4. Vertical potential distribution in the Si film for different channel lengths and drain biases.

shown in Fig. 4 and excellent agreements can be seen. These indicate that the errors caused by the artificial boundary potentials in Region I and Region III are negligibly small. In our analytic modeling, the effects of free carriers are neglected in the subthreshold region and this assumption is proven to be valid for short-channel thin-film SOI MOSFET's even when the drain bias is large.

III. The Threshold-Voltage Model

From Section II, the surface potential distribution at the front interface can be further rewritten in terms of terminal voltages as

$$\Phi_f^{II}(x) = -\frac{qN_B}{2\epsilon_{si}}x(L-x) + V_{bi} + \frac{x}{L}V_{ds} + \sum_{m=1}^{\infty}(V'_{gs}\cdot G_f^m + V'_{BS}\cdot G_b^m + P^m)\sin k_m x \tag{7}$$

where

$$G_f^m = [1-(-1)^m]\frac{R_1^m}{d_0^m}\left[\frac{2}{m\pi\cosh k_m t_{of}} + \sum_{n=1}^{\infty}\frac{t_{mn}^{I}}{(n-0.5)\pi}\left[(-1)^{n+1} - \frac{1}{(n-0.5)\pi}\right]\right]$$

$$G_b^m = [1-(-1)^m]\frac{R_2^m}{d_0^m}\left[\frac{2}{m\pi\cosh k_m t_{ob}} + \sum_{n=1}^{\infty}\frac{t_{mn}^{III}}{(n-0.5)\pi}\left[(-1)^{n+1} - \frac{1}{(n-0.5)\pi}\right]\right]$$

$$P^m = \frac{1}{d_0^m}\left[[1-(-1)^m]\frac{qN_BL^2}{2\epsilon_{si}}\frac{4(R_1^m+R_2^m)}{(m\pi)^3} + T^m[V_{bi}(1-(-1)^m)+V_{ds}(-1)^{m+1}]\right]$$

$$T^m = \sum_{n=1}^{\infty}[R_1^m t_{mn}^{I} + R_2^m t_{mn}^{III}][(n-0.5)\pi]^{-2} - 2(R_1^m+R_2^m)/m\pi$$

$$R_1^m = -1 - \frac{\epsilon_{si}\tanh k_m t_{ob}}{\epsilon_{ox}\tanh k_m t_{si}}$$

$$R_2^m = -\frac{\epsilon_{si}\tanh k_m t_{of}}{\epsilon_{ox}\sinh k_m t_{si}}.$$

The Fourier coefficients in (7) are further checked if the first coefficient $m = 1$ is the dominant term. It is shown that the coefficient of the first term is about ten times larger than the next significant coefficient when the drain bias is small. However, a large error may be produced for a large-drain bias if the first-term approximation is used. It is seen that the first coefficient is not even the dominant one in some cases. Another problem of using the first-term approximation is that it will lead to an erroneous result for the position of the minimum surface potential. Therefore, the series solution is kept for the following derivations without losing accuracy.

Differentiating (7) with respect to x, the position of the minimum surface potential can be obtained. Note that the location of the minimum surface potential (x_{min}) can only be solved by iteration since no explicit solution for x_{min} can be obtained. The calculated x_{min} is then substituted into (7) and the minimum surface potential is obtained as

$$\Phi_{f,min}^{II} = -\frac{qN_B}{2\epsilon_{si}}x_{min}(L-x_{min}) + V_{bi} + \frac{x_{min}}{L}V_{ds} + V'_{gs}\sum_{m=1}^{\infty}G_f^m \sin k_m x_{min} + V'_{BS}\sum_{m=1}^{\infty}G_b^m \sin k_m x_{min} + \sum_{m=1}^{\infty}P^m \sin k_m x_{min}. \quad (8)$$

It is clearly seen that the relation between the minimum surface potential and the external bias can be deduced from (8) when the minimum surface potential reaches the inversion condition $\phi_{f,inv}$ as the applied gate bias is equal to the threshold voltage. Setting $\Phi_{f,min}^{II} = \phi_{f,inv}$, the threshold voltage can be analytically expressed as

$$V_T^f = V_{fb,f} + \left\{\phi_{f,inv} + \frac{qN_B}{2\epsilon_{si}}x_{min}(L-x_{min}) - V_{bi} - \frac{x_{min}}{L}V_{ds}\right\}\left[\sum_{m=1}^{\infty}G_f^m \sin k_m x_{min}\right]^{-1} - \sum_{m=1}^{\infty}(V'_{BS}\cdot G_b^m + P^m)\sin k_m x_{min}\cdot\left[\sum_{m=1}^{\infty}G_f^m \sin k_m x_{min}\right]^{-1}. \quad (9)$$

Note that an initial guess for the threshold voltage is used to calculate the location of the minimum surface potential, then x_{min} is substituted into (9) to solve the threshold voltage, and the iteration procedure is continued until convergence is reached. It is found that the number of iterations is small and the computation time used is short. In order to compare the results of the developed analytic threshold-voltage model with those of 2D numerical analysis, the threshold voltage derived by the 2D numerical analysis is defined by the drain current as follows: the threshold voltage of a long-channel (10-μm) SOI MOSFET is extracted by checking the $\Phi_{f,min}^{II} - V_{gs}$ relation corresponding to the I_{ds}–V_{gs} characteristics from 2D numerical analysis. The normalized drain current corresponding to $\Phi_{f,min}^{II} = 2\,\phi_{fp}$ is taken as the reference current, then the threshold voltage of a shorter-channel device is extracted by equating the normalized drain current to the specified reference current.

The calculated threshold voltages using (9) for a SOI MOSFET with 70-mn Si film, 15-nm front gate oxide, and 320-nm bottom oxide are compared with the 2D numerical analysis in Fig. 5(a) with the back-gate bias as a parameter. It is clearly seen that excellent agreements between our model and the 2D numerical analysis are obtained and poor agreements for Young's model are demonstrated. Comparisons of the calculated threshold voltages as a function of the effective channel length with the drain as a parameter are shown in Fig. 5(b), in which the thickness of the front gate oxide, the Si film, and the bottom oxide remain the same. Fig. 5(b) shows that good agreements are also obtained for devices with channel length as short as 0.4 μm. However, the discrepancy for shorter channel length devices (for example, $L_{eff} = 0.3$ μm) operated with larger drain bias is mainly due the serious drain-induced barrier-lowering effect at the bottom Si/SiO_2 interface, as checked by 2D numerical analysis. It is clearly seen that the underestimation of the drain-induced barrier-lowering effect in [5] results in a smaller threshold-voltage roll-off for shorter effective channel lengths.

The calculated threshold voltages using our model as a function of the effective channel length with the thickness of the front gate oxide as a parameter are compared with those using 2D numerical analysis in Fig. 6. It is easily seen that the developed threshold-voltage model agrees well with the 2D numerical analysis. Similar good agreement can also be observed from Fig. 7, where the threshold voltage is plotted as a function of the effective channel length with the thickness of the Si film as a parameter. The slight discrepancy for shorter channel devices is attributed to the easy penetration of the source/drain built-in electric fields at the back Si surface. From Figs. 6 and 7, it is clearly seen that our analytic model agrees with 2D numerical analysis for different doping concentrations in the Si film. It is concluded that the penetration of the source/drain electric fields is more likely to occur at the back Si surface when the doping concentration in the Si film is lower or when the channel length is shorter. This

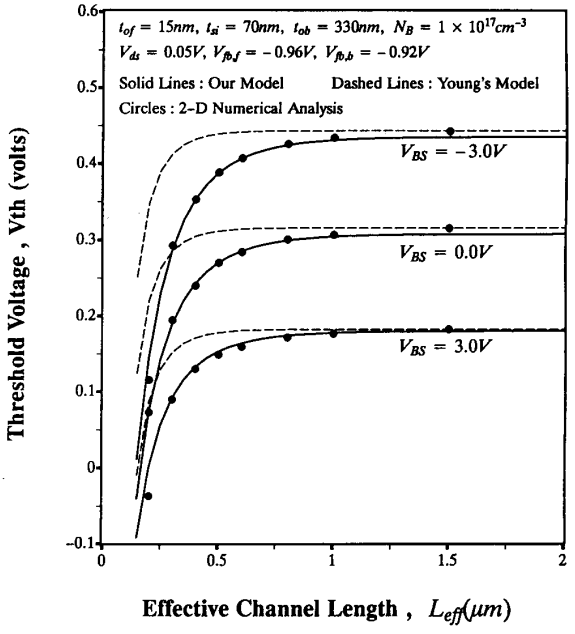

(a)

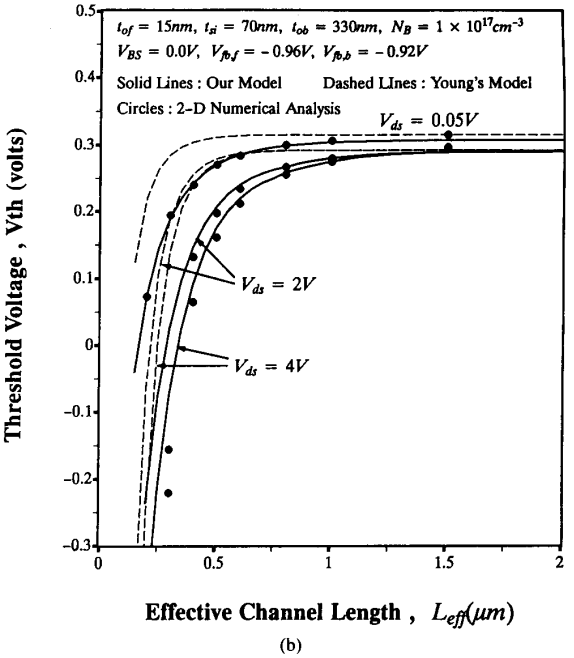

(b)

Fig. 5. Calculated threshold voltages as a function of the effective channel length for different models or method (a) with the back-gate bias as a parameter and (b) with the drain bias as a parameter.

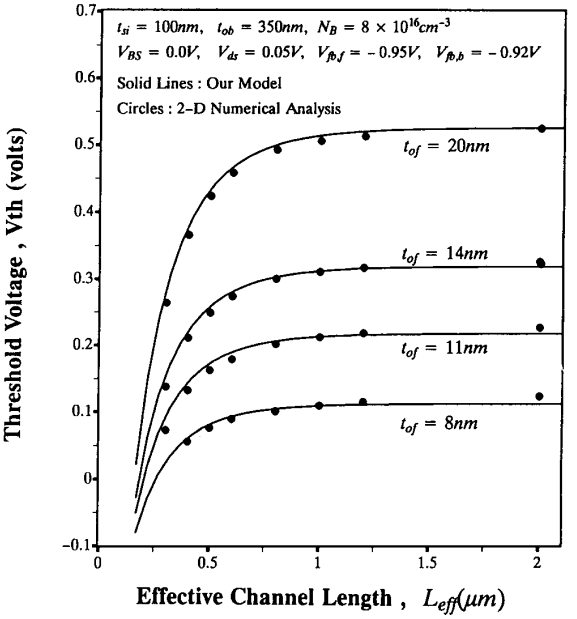

Fig. 6. Calculated threshold voltages as a function of the effective channel length with the thickness of the front-gate oxide as a parameter.

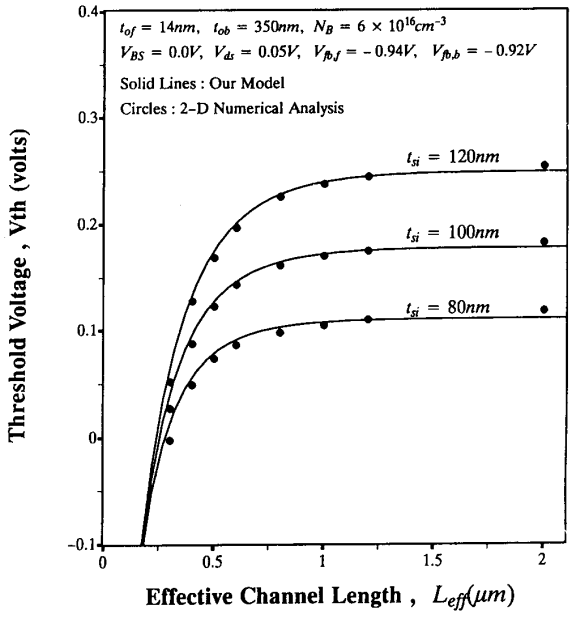

Fig. 7. Calculated threshold voltages as a function of the effective channel length with the thickness of the Si film as a parameter.

effect can be improved by increasing the doping concentration at the back Si surface using ion implantation. It should be noted that the condition of the fully depleted device can be estimated by the one-dimensional analysis of the Poisson's equation, as derived in [4]. From the above comparisons, it is clearly demonstrated that the developed threshold-voltage model can accurately predict the threshold behavior of fully depleted short-channel SOI MOSFET's with different structure parameters under different applied biases.

IV. Conclusion

The exact solution of the 2D Poisson's equation has been analytically derived by a three-zone Green's function solution technique with the suitable boundary con-

ditions in different zones. The accuracy of the derived 2D potential distribution in the Si film has been verified by 2D numerical analysis. This indicates that the uses of the artificial linear potentials at the oxide edges are sufficient for solving the 2D Poisson's equation. Based on the accurate 2D potential distribution, the analytic potential distribution at both front and back surfaces in the Si film are derived. It is shown that the location of the minimum surface potential can only be solved iteratively and the computation effort taken by the iteration procedure is small. Moreover, an analytic threshold-voltage model is derived and compared with the 2D numerical analysis. It is clearly shown that good agreements are obtained between the developed threshold-voltage model and the 2D numerical analysis for wide ranges of device structure parameters and applied biases. The accurate analytic threshold-voltage model can provide a fast physical analysis of the short-channel effect and further give the scaling rule for deep-submicrometer thin-film SOI MOSFET's in ULSI.

REFERENCES

[1] J.-P. Colinge and T. I. Kamins, "CMOS circuits made in thin SIMOX film," *Electron Lett.*, vol. 23, p. 1162, Oct. 1987.

[2] K. Terrill, J. Woo, and P. K. Vasudev, "Design and performance of submicron MOSFET's on ultra-thin SOI for room temperature and cryogenic operation," in *IEDM Tech. Dig.*, 1988, p. 294.

[3] J.-P. Colinge, "Thin-film SOI technology: The solution to many submicron CMOS problems," in *IEDM Tech. Dig.*, 1989, p. 817.

[4] S. Veeraraghavan and J. G. Fossum, "Short-channel effects in SOI MOSFET's," *IEEE Trans. Electron Devices*, vol. 36, no. 3, p. 522, Mar. 1989.

[5] K. K. Young, "Short-channel effects in fully depleted SOI MOSFET's," *IEEE Trans. Electron Devices*, vol. 36, no. 2, p. 399, Feb. 1989.

[6] K. N. Ratnakumar and J. D. Meindl, "Short-channel MOSFET threshold voltage model," *IEEE J. Solid-State Circuits*, vol. SC-17, no. 5, p. 937, 1982.

[7] J. C. S. Woo, K. W. Terrill, and P. K. Vasudev, "Two-dimensional analytic modeling of very thin SOI MOSFET's," *IEEE Trans. Electron Devices*, vol. 37, no. 9, p. 1999, Sept. 1990.

[8] P.-S. Lin and C.-Y. Wu, "A new approach to analytically solving the 2-D Poisson's equation and its application in short-channel MOSFET modeling," *IEEE Trans. Electron Device*, vol. ED-34, no. 9, p. 1947, Sept. 1987.

[9] S. P. Chin and C. Y. Wu, "A new two-dimensional model for the potential distribution of short gate-length MESFET's and its applications," *IEEE Trans. Electron Devices*, vol. 39, no. 8, p. 1928, Aug. 1992.

[10] ——, "A new methodology for two-dimensional numerical simulation of semiconductor devices," *IEEE Trans. Computer-Aided Des.*, vol. 11, no. 12, p. 1508, Dec. 1992.

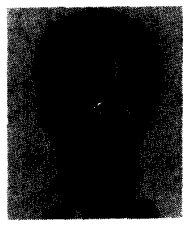

Jwin-Yen Guo (S'91) was born in Kaoshong, Taiwan, ROC, in 1963. He received the B.S.E.E. degree from the Department of Electrical Engineering, National Taiwan University, Taipei, Taiwan, in 1985 and the M.S.E.E. degree from the Institute of Electronics, National Chiao-Tung University, Hsinchu, Taiwan, in 1987.

He is presently working towards the Ph.D. degree in the Institute of Electronics, National Chiao-Tung University. His current research interests are in the characterization and modeling of thin-film field-effect transistors.

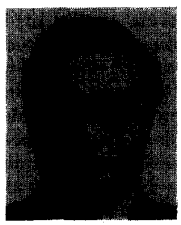

Ching-Yuan Wu (M'72) was born in Taiwan, Republic of China, on March 18, 1946. He received the B.S. degree from the Department of Electrical Engineering, National Taiwan University, Taiwan, Republic of China, in 1968, and the M.S. and Ph.D. degrees from the State University of New York (SUNY) at Stony Brook, in 1970 and 1972, respectively.

During the 1972–1973 academic year, he served as Lecturer at the Department of Electrical Sciences, SUNY, Stony Brook. During the 1973–1975 academic years, he was a Visiting Associate Professor at National Chiao-Tung University (NCTU), Taiwan, Republic of China. In 1976, he became a Full Professor in the Department of Electronics and the Institute of Electronics, NCTU. In NCTU, he had been the Director of Engineering Laboratories and Semiconductor Research Center, during 1974–1980; the Director of the Institute of Electronics, during 1978–1984; and the Dean, College of Engineering, during 1984–1990. He was a principal investigator of the National Electronics Mass Plan—Semiconductor Devices and Integrated- Circuit Technologies, during 1976–1979, and had been a Coordinator of the National Microelectronics Research and High-Level Man-Power Education Committee, National Science Council, Republic of China, during 1982–1988. He has been a Research Consultant for the Electronics Research and Service Organization (ERSO), ITRI; a member of the Academic Review Committee, the Ministry of Education; and the chairman of the Technical Review Committee on Information and Microelectronics Technologies, the Ministry of Economic Affairs. His research activities have been in semiconductor device physics and modelings, integrated-circuit designs and technologies. His present research areas focus on the developments of efficient 2D and 3D simulators for deep-submicrometer semiconductor devices, design rules, and optimization techniques for deep-submicrometer CMOS devices, and key technologies for deep-submicrometer CMOS devices. He has published over 160 papers in the semiconductor field and has served as a reviewer for internal journals such as IEEE ELECTRON DEVICE LETTERS, IEEE TRANSACTIONS ON ELECTRON DEVICES SOLID-STATE ELECTRONICS, etc.

He received the Academic Research Award in Engineering from the Ministry of Eduction (MOE), in 1979; the Outstanding Scholar Award from the Chinese Educational and Cultural Foundation, in 1985. He has received the outstanding research Professor fellowship from the Ministry of Education and the National Science Council (NSC), Republic of China, during 1982–1993. He has also received the Distinguished Engineering Professor Gold Medal Award from the Chinese Engineering Society in 1992.

Dr. Wu is a member of the Honorary Editor Advisory Board of Solid-State Electronics and is a board member of the Chinese Engineering Society.